Accident Analysis and Prevention 106 (2017) 285–296

Contents lists available at ScienceDirect

Accident Analysis and Prevention

journal homepage: www.elsevier.com/locate/aap

Exploring the mechanisms of vehicle front-end shape on pedestrian head injuries caused by ground impact

Sha Yin[a,b], Jiani Li[a,b], Jun Xu[a,b,*]

[a] Department of Automotive Engineering, School of Transportation Science and Engineering, Beihang University, Beijing, 100191, China
[b] Advanced Vehicle Research Center (AVRC), Beihang University, Beijing, 100191, China,

ARTICLE INFO

Keywords:
Pedestrian–vehicle accident
Front-end shape
Head injury
Head–ground impact

ABSTRACT

In pedestrian–vehicle accidents, pedestrians typically suffer from secondary impact with the ground after the primary contact with vehicles. However, information about the fundamental mechanism of pedestrian head injury from ground impact remains minimal, thereby hindering further improvement in pedestrian safety. This study addresses this issue by using multi-body modeling and computation to investigate the influence of vehicle front-end shape on pedestrian safety. Accordingly, a simulation matrix is constructed to vary bonnet leading-edge height, bonnet length, bonnet angle, and windshield angle. Subsequently, a set of 315 pedestrian–vehicle crash simulations are conducted using the multi-body simulation software MADYMO. Three vehicle velocities, i.e., 20, 30, and 40 km/h, are set as the scenarios. Results show that the top governing factor is bonnet leading-edge height. The posture and head injury at the instant of head ground impact vary dramatically with increasing height because of the significant rise of the body bending point and the movement of the collision point. The bonnet angle is the second dominant factor that affects head–ground injury, followed by bonnet length and windshield angle. The results may elucidate one of the critical barriers to understanding head injury caused by ground impact and provide a solid theoretical guideline for considering pedestrian safety in vehicle design.

1. Introduction

Pedestrian safety remains a priority in vehicle design and pedestrian protection is a critical evaluation indicator in consumer and legislative tests (EEVC, 1998; Euro-NCAP, 2013). The global road safety report released by the World Health Organization in 2015 (WHO, 2015) indicated that approximately 1.25 million people had died from vehicle accidents, and nearly half of the fatalities were vulnerable road users (VRUs), including pedestrians (22%), cyclists (4%), and motorcyclists (23%). In China, approximately one quarter of the total road fatalities involve VRUs. Furthermore, a study on 328 fatal pedestrian cases found that head injury might lead to approximately 84% chance of death (including those with multiple death causation), thereby indicating that head injury was the dominant cause of pedestrian death (Belingardi and Chiandussi, 2011; Hefny et al., 2014).

Therefore, numerous efforts have been exerted to determine the mechanisms of various types of pedestrian injury to improve vehicle safety evaluation and design. Among the universal factors, such as vehicle velocity (Cuerden and Richards 2007; Poorfakhraei et al., 2014; Yan et al., 2015), pedestrian initial stance (Simms and Wood 2006; Elliott et al., 2012), protective effect of the helmet (Oida et al., 2015; Demarco et al., 2016), and impact location (Yang and Yao, 2005; Xu et al., 2015), vehicle front-end shapes have been studied extensively (Han et al., 2012; Lyons and Simms, 2012; Crocetta et al., 2015; Sankarasubramanian et al., 2015) because this factor can be optimized directly to help avoid collisions and reduce the possibility of serious injuries.

In general, head injuries stem from three major processes: the first contact between the lower limbs of the pedestrian and the bonnet, the second contact between the head/shoulder/pelvis of the pedestrian and the engine hood/windshield, and the final contact between the head/shoulder of the pedestrian and the ground (Roudsari et al., 2005). The pedestrian–vehicle interaction is highly dependent on vehicle profile, which has triggered many pioneering works. Yan et al. (Yan et al., 2015) found that the head injury criterion (HIC) in van collisions was 1.3–2.2 times that in small car and sedan collisions within a speed range of 38–60 km/h. The major difference was attributed to the front-ends of various vehicle types. The Total Human Model of Safety (Iwamoto et al., 2002) and four vehicle models with different front-ends were used to analyze the kinematic response of pedestrians, with HIC and rib deflection as injury indicators (Han et al., 2011). The results showed that a short vehicle engine hood and a large windshield area considerably reduced the risk of lethal damage. Furthermore, Lyons and

* Corresponding author at: Department of Automotive Engineering, School of Transportation Science and Engineering, Beihang University, Beijing, 100191, China.
E-mail address: junxu@buaa.edu.cn (J. Xu).

http://dx.doi.org/10.1016/j.aap.2017.06.005
Received 30 November 2016; Received in revised form 5 June 2017; Accepted 6 June 2017
Available online 24 June 2017
0001-4575/

Simms (Lyons and Simms, 2012) probed into the influence of windshield angle, stiffness characteristics, and friction coefficient on head injury risk during the primary impact between the head and the windshield. They found that increasing windshield angle reduced the peak value of head linear acceleration by 7% and head angular acceleration by 18%. Simultaneously, a large friction coefficient would generate high head acceleration. In addition, full-scale vehicle pedestrian impact tests with different vehicles were performed using both PMHS and the Polar-II dummy (Kerrigan et al., 2005; Subit et al., 2008; Kerrigan et al., 2012), verifying the effect of vehicle front-end on pedestrian head injury during contact with vehicle.

By contrast, limited research has focused on head injuries induced by ground impact because of the diverse kinematic processes and the complicated mechanism of impact with the ground. Kendall et al. (Kendall et al., 2006) compared injuries from head–engine hood and head–ground contact and found that the former was more severe at low speed, whereas both types of injury were extremely severe at high speed. They also pointed out that the secondary injury caused by the ground was always more severe in collisions with sport utility vehicles (SUVs). Hamacher et al. (Hamacher et al., 2012) found that direct head–ground contact tended to occur when a pedestrian was struck by a vehicle with a high leading edge and large bonnet and windshield angles. A simulative study was also conducted to determine the influence of vehicle front-end profile on secondary impact injury. The results showed that mid-size vehicles with a low leading edge and SUVs with a high leading edge could prevent direct contact between the head and the ground, whereas mid-size vehicles with a high leading edge and SUVs with a low leading edge always led to direct contact; the reasons for these findings remained unclear (Gupta and Yang, 2013). A series of studies that focused on secondary impact (head–ground) injury was conducted by Simms et al. In 2006, they found that the head impact point location and injury were predictable with the variation in pedestrian initial stance during the primary impact (head–vehicle contact) but unpredictable during the secondary impact (Simms and Wood, 2006). In 2011, Simms et al. (Simms et al., 2011) performed simulations to investigate the influence of bonnet leading edge. The results showed that vehicles with a high bonnet leading edge, such as SUVs, tended to cause the head to strike the ground first. Six circulatory impact mechanisms were suggested. To comprehensively study the head–ground impact phenomenon and validate the usability of the six impact mechanisms, Simms (Crocetta et al., 2015) adopted more representative vehicle types, a wider speed range, and more varied pedestrian initial stances.

However, current studies have not yet identified dominant factors, particularly for the effect of vehicle front-end shape on head injuries caused by secondary impact, and thus, the mechanism of head injuries remains unclear. To bridge this gap, the current work comprehensively conducts a simulative investigation on injuries caused by head–ground contact. In Section 2, simulative crash scenarios, including pedestrian and vehicle models, are established, and a parametric study matrix is designed. In Section 3, the rotation angle is suggested to be a dominant variable in head–ground contact description. In Section 4, comprehensive parametric discussions are presented to indicate the mechanism of head–ground impact injuries.

2. Methods

2.1. Human model

The 50th% mid-size male pedestrian model (Automotive 2013) was used in the impact with the parameterized vehicle models. The pedestrian model consisted of 52 rigid bodies presented in 7 configuration branches and an outer surface described by 64 ellipsoids and 2 planes. The model was verified on both segment and full-body levels with a volunteer and post-mortem human subject test data (Automotive 2013). The comparison between full-scale impact tests and computer simulations in terms of the kinematics of pedestrians, force during bonnet impact, and acceleration of body segments was evaluated and further validated the pedestrian model during the interaction with the vehicle (Yang et al., 2000). Moreover, to ensure the feasibility of pedestrian model after vehicle impact, Yao et al. (Yao et al., 2008) used the MADYMO pedestrian model to reconstruct 10 real accidents and found a good correspondence between simulations and collision data in terms of pedestrian wrap-around distance and pedestrian throw distance. However, the capability of the pedestrian model to predict injury from ground impact has not been verified. And it is a limitation of this study.

2.2. Vehicle models

The vehicle model was established based on an actual vehicle model, namely, the Toyota Camry. This basic vehicle model weighed 1800 kg and exhibited the following front-end dimensional parameters: a bonnet leading edge of 0.8 m, a bonnet length of 1.1 m, a bonnet angle of 10°, and a windshield angle of 25°. The loading and unloading curves of the vehicle materials were obtained from the European New Car Assessment Program subsystem tests (Martinez et al., 2007). In particular, the windshield was divided into three sections for modeling by considering the different stiffness levels of head impact locations on the windshield. The stiffness levels of the windshield sections were obtained from (Mizuno and Yonezawa 2001).

The contact type between pedestrian and vehicle was set as combined contact, and a friction coefficient of 0.3, which was verified in a previous research (Simms and Wood 2006), was set for pedestrian–vehicle contact. Pedestrian–road contact was set as slave contact, and only pedestrian contact characteristics were used. The friction coefficient of pedestrian–road contact was set as 0.58 based on the test results of (Wood et al., 2000).

2.3. Impact scenarios

The kinematic response of a pedestrian and the posture at pedestrian–ground impact would be extremely complicated and varied given the high flexibility of the human model, which was connected by 53 joints. Therefore, defining the impact scenarios with considerable influence on the simulation results is necessary. The human model in this study was deliberately arranged such that it would be struck by the vehicle exactly on its middle section. The pedestrian would remain standing until it was struck from the lateral side. Such scenario occurs frequently at a cross intersection on a road (Yan et al., 2011), as illustrated in Fig. 1. Since the simulations were analyzed individually, only single initial stance and single walking speed were considered in this study in order to attain a reasonable analysis time. Actually, the simulation result is sensitive to these two factors (Crocetta et al., 2015) and the pedestrian stance defined here is most common rather than most dangerous.

The impact velocities of 20, 30, and 40 km/h were selected to represent a wide range of typical pedestrian–vehicle impact speeds (Simms and Wood, 2009). When impact velocity exceeds 40 km/h, the pedestrian will suffer more seriously from the impact with the vehicle than from that with the ground (Feng et al., 2013), and death mainly results from head–vehicle contact instead of head–ground impact. In addition, a constant deceleration of 0.8 g was adopted for the brake effect by setting the friction coefficient of vehicle–road contact as 0.8, similar to the strategy used by (Xu et al., 2015; Xu et al., 2016).

2.4. Injury evaluation index

HIC is widely accepted for assessing the severity of head injuries. The HIC_{15} value of 700 represents a 5% risk of receiving a severe injury. Head injury from pedestrian ground impact in partial simulations are assessed using both HIC_{15} and averages angular acceleration. The comparison between these two injury evaluation indexes is shown in Fig. 2. It is interesting to find that HIC_{15} and averaged angular acceleration are well correlated, similar to the results in (Kerrigan et al., 2012). Therefore, choosing HIC_{15} to describe head injury is appropriate

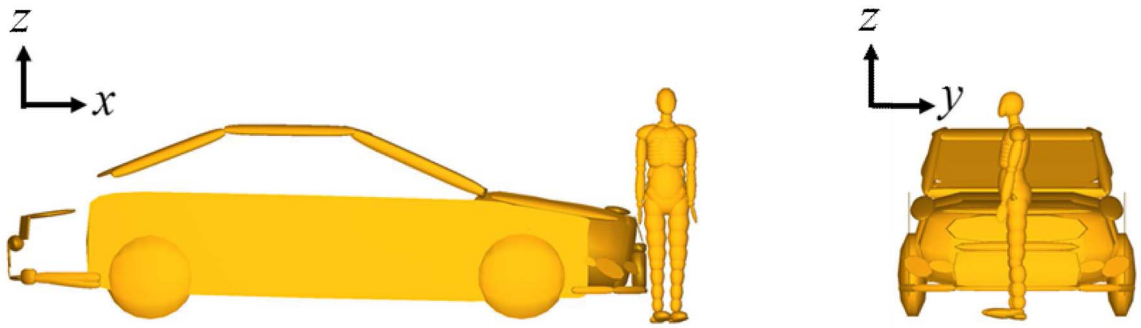

Fig. 1. Typical impact scenario and coordinate system of the impact model.

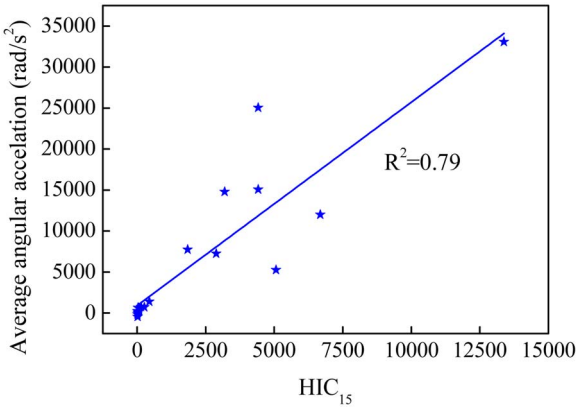

Fig. 2. Averaged angular acceleration vs. HIC_{15} for partial simulations.

and sufficient in this study.

A typical head acceleration–time curve during a pedestrian–vehicle collision is illustrated in Fig. 3, where two distinguishable peaks are observed at the instances of the primary and secondary impacts. In the illustrated case, the HIC_{15} values calculated from the acceleration values for the two peaks were 678.061 and 3044.92.

2.5. Design of parametric study

The dimensional parameters that described vehicle front-end shape would immediately change contact posture with the vehicle and influence the severity of the injury obtained from the primary impact. The subsequent projector trajectory and pedestrian posture would vary correspondingly. Furthermore, different kinematic responses would lead to significant variations in pedestrian stance and the touching region of the body at the instant of ground contact, which would finally affect injury risk during the secondary impact. Evidently, designing a parametric study matrix for vehicle front-end shape is important. To quantify and simplify the vehicle model, four main characteristic parameters were selected: bonnet leading edge height (H), bonnet length (L), bonnet angle (α), and windshield angle (θ). These parameters were able to briefly draw the outline of the vehicle front-end, as shown in Fig. 4.

The values of these four dimensional parameters were recorded regularly in their respective value areas. Table 1 shows the parametric matrix that consists of these reasonable values. The value ranges of H (0.5–1.0 m), L (0.5–1.5 m), and α (5° − 30°) were set based on (Crocetta et al., 2015), whereas the range of θ (20° − 45°) was obtained from (Lyons and Simms, 2012). The original vehicle model mentioned earlier also conformed to these requirements and was regarded as the baseline. From the parametric matrix, the vehicle models with different front-end shapes were parametrically built based on the original model using MADYMO software (Automotive, 2013). To consider the coupling influence of double variables, 105 vehicle models were built by coupling H and one of the other three parameters with the two remaining parameters kept the same as the baseline. Geometrically unreasonable models were ruled out.

A total of 315 simulations were conducted for 105 geometric vehicle models at three speeds (i.e., 20, 30, and 40 km/h) to investigate the influences of vehicle structure and speed on head injuries from pedestrian–ground impact.

3. Results

3.1. Body rotation angle at the instant of ground impact

The rotation angle of the upper body around the y-axis from the initial stationary stance to the final impact with the ground is defined as the rotation angle (γ), as shown in Fig. 5. This angle can briefly describe the pedestrian posture at the instant of ground impact, which is directly related to the severity of the injury from head–ground impact. The

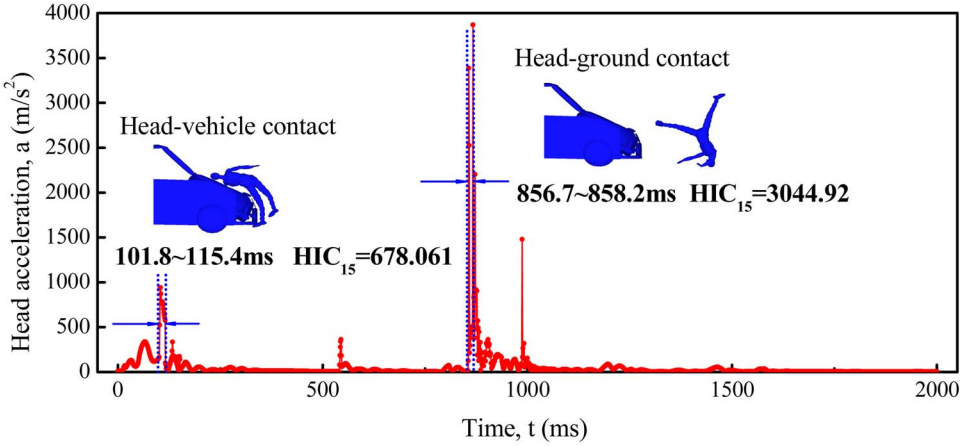

Fig. 3. Resultant head acceleration of a pedestrian when struck at 40 km/h. Head–vehicle impact and head–ground impact are indicated with HIC_{15} values of 678.061 and 3044.92, respectively.

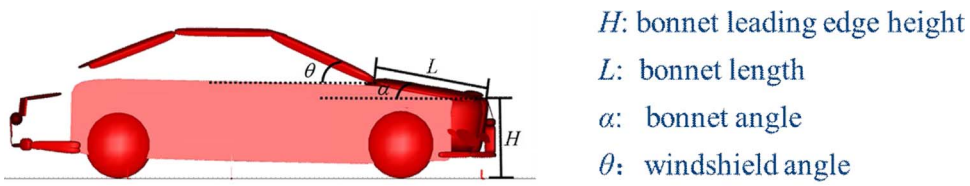

Fig. 4. Dimensional parameters of vehicle front-end structure. Bonnet leading edge height (H) bonnet length (L), bonnet angle (α), and windshield angle (θ) are indicated.

Table 1
Parametric matrix that consists of the dimensional parameters of vehicle front-end.

Bonnet leading edge height H (m)	Bonnet length L (m)	Bonnet angle α	Windshield angle θ
0.5	0.5	5°	20°
0.6	0.7	10°	25°
0.7	0.9	15°	30°
0.8	1.1	20°	35°
0.9	1.3	25°	40°
1.0	1.5	30°	45°

value of γ varies frequently because it is related to multiple factors, such as impact speed (v), vehicle front-end structure, and pedestrian initial stance. In this study, γ is regarded as a quantitative index of pedestrian–ground impact posture to investigate the mechanisms of vehicle profile parameters and impact velocity on landing posture and injury severity. As shown in Fig. 5, all γ values obtained from the simulation results can be divided into four sections: Section I ($0^\circ < \gamma < 90^\circ$), Section II ($90^\circ < \gamma < 180^\circ$), Section III ($180^\circ < \gamma < 270^\circ$), and Section IV ($270^\circ < \gamma < 360^\circ$).

3.2. Coupling effect of bonnet leading edge height and bonnet angle

The height of the bonnet leading edge (H) has been generally studied as a governing factor of pedestrian–ground impact injury (Otte and Pohlemann, 2001; Gupta and Yang, 2013). However, a single variable H may not illustrate the complicated head–ground impact process. In this case, the coupling effect with the bonnet leading edge height is comprehensively studied.

A series of parameterized vehicle front-end models varying in H and α values was established and then simulated in virtual crashes at impact speeds of 20, 30, and 40 km/h to determine the coupling effect of H and α at different speeds.

As shown in Fig. 6(a), the variation range of γ resulting from H and α expands with increasing impact velocity from 37.25°–126.06° (Sections I and II) at 20 km/h, 55.01°–237.80° (Sections I, II, and III) at 30 km/h, to 45.27°–305.41° (Sections I, II, III, and IV) at 40 km/h. This phenomenon indicates that a high speed increases the sensitivity of γ to H and α. At 20 km/h, either H or α can significantly influenceγ. At 30 km/h, both H and α contribute to the variation of γ. At 40 km/h, H evidently plays a leading role, whereas α slightly influencesγ, as shown in Fig. 6(a).

3.3. Coupling effect of bonnet leading edge height and bonnet length

Similarly, an extensive parametric study was conducted to elucidate the coupling effect of H and L on pedestrian–ground impact configuration described byγ, as illustrated in Fig. 6(b). As velocity increases, the variation range of γ arises from$H$, and L expands gradually from 40.11°–99.13° (Sections I and II) at 20 km/h, 30.37°–147.83° (Sections I and II) at 30 km/h, to 40.11°–293.95° (Sections I, II, III, and IV) at 40 km/h because of the increased sensitivity of γ to H and L. At 20 km/h, neither H nor L can effectively influence the values of γ. A similar phenomenon can be observed at 30 km/h. At 40 km/h, H mainly determines the results of γ, whereas the alteration of L is demonstrated with minimal effect on the consequences.

3.4. Coupling effect of bonnet leading edge height and windshield angle

Fig. 6(c) shows the coupled effect of H and θ on γ. Similarly, the variation range of γ resulting from H and θ expands gradually from 17.19°–85.95° (Section I) at 20 km/h, 39.54°–205.13° (Sections I, II, and III) at 30 km/h, to 44.69°–297.39° (Sections I, II, III, and IV) at 40 km/h. The values of γ at 20 km/h are generally stable with minimal fluctuation. At 30 km/h, H and θ contribute to the distribution of γ. In particular, a peak value of γ appears at H = 0.6 m and θ of approximately 40°, as shown in Fig. 7, which illustrates six post-impact motion processes (H = 0.6 m, θ ranging from 20° to 45°). In these cases, a small θ (20° − 35°) tends to generate a similarly small γ because a low impact point produces a noticeable bonnet obstacle to pedestrian kinetics during rotation. A large θ (20° − 35°) can raise the impact point, reduce the effect of the obstacle, and consequently, generate a larger γ. However, the circumstances where θ influences γ dramatically are accidental, i.e., they cannot represent the general situation. In general, the governing factor H dominates the value of γ compared with θ at 40 km/h.

4. Discussion

Double factors-no repeated variance analysis was used and Table 2 listed the significance levels of vehicle front-end design factors on

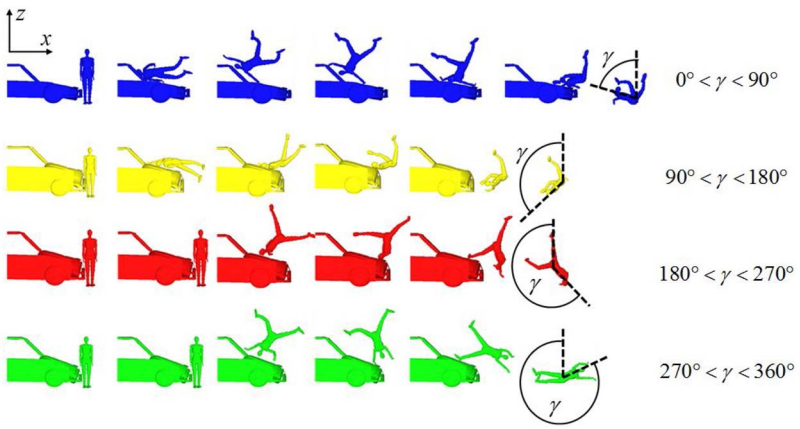

Fig. 5. Description of the rotation angles in four sections. $0^\circ < \gamma < 90^\circ$in Section I, $90^\circ < \gamma < 180^\circ$in Section II, $180^\circ < \gamma < 270^\circ$in Section III, and $270^\circ < \gamma < 360^\circ$ in Section IV.

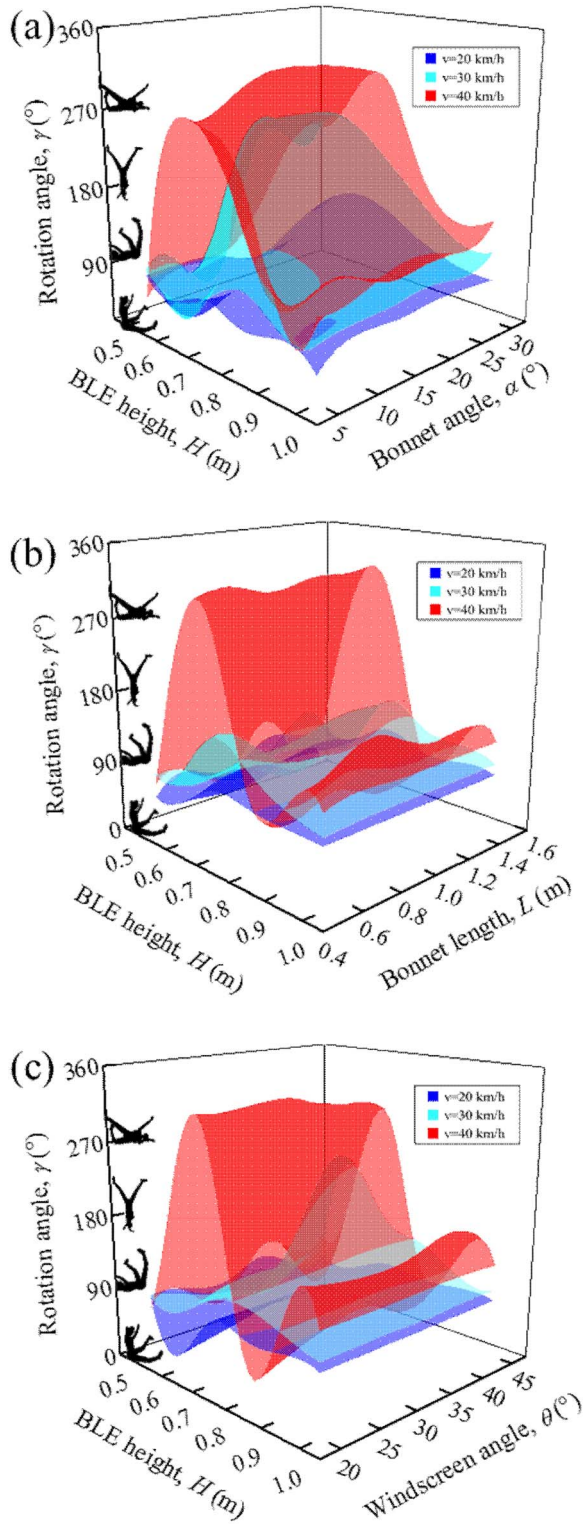

Fig. 6. (a) Coupling effect of H and α on γ at all impact speeds (20, 30, and 40 km/h). (b) Coupling effect of H and L on γ at all impact speeds (20, 30, and 40 km/h). (c) Coupling effect of f H and θ on γ at all impact speeds (20, 30, and 40 km/h). The red, light blue, and dark blue surfaces represent the cases at 40, 30, and 20 km/h, respectively. (For interpretation of the references to colour in this figure legend, the reader is referred to the web version of this article.)

rotation angle at 40 km/h. Smaller P-value represents more significant influence. It can be obviously observed that the top governing factor is bonnet leading-edge height.

For a more comprehensive analysis, multiple linear regression analysis has been made based on cases at 40 km/h. The following is the regression model and we added coefficient of 100 before the variables to get a more reasonable result:

$$\log(100\gamma) = \beta_0 + \beta_H \log(100H) + \beta_\alpha \log(100\alpha) + \beta_L \log(100L) + \beta_\theta \log(100\theta) \quad (1)$$

Table 3 lists brief information on the fitted coefficients and p-values for the variables in the regression model. The elasticity of γ to H, α, L, θ are respectively −2.066, 0.037, 0.236, 0.008, indicating that γ is more sensitive to H than α, L, θ. The difference in the influence capability of the dimensional parameters is attributed to various influence mechanisms.

4.1. The influence mechanism of bonnet leading edge height on rotation angle

Fig. 8 illustrates the detailed kinematic response process for the case of 40 km/h where vehicle front-end shape varies with H and the other three parameters are maintained at baseline values. It can be observed that γ varies dramatically with different H values. The γ values generated by H values of 0.6 m (γ = 246.39°) and 0.7 m (γ = 292.23°) are larger than those generated by H values of 0.8 m (γ = 74.49°), 0.9 m (γ = 97.41°), and 1.0 m (γ = 114.60°). The comparison of the 86 mm images of cases H = 0.6 m and H = 1.0 m (Fig. 9) shows that when a vehicle with H = 0.6 m strikes a pedestrian, the body bends at a lower impact point, which increases the moment generated by the gravity of the upper body, facilitates rotation motion, and consequently, increases the rotation angle γ at the instant of pedestrian–ground impact. However, γ does not decrease proportionately as H increases. When H = 0.5 m, the long distance from the head impact point to the bonnet ledge leads to a serious obstacle caused by the bonnet and finally generates a smaller γ (40.11°) than that when H = 0.6 m (γ = 246.39°). Otherwise, when H > 0.8 m, the rotation angles at the instant of separation between pedestrians and vehicles are similar (nearly 90°). Subsequently, the increased rotation angles are positively correlated with H (Fig. 8). By contrast, the location of the head–vehicle impact point with a higher bonnet moves from the windshield to the bonnet. Different windshield material characteristics lead to various kinematic responses. All these factors contribute to the irregular fluctuation of γ as H increases. In general, H significantly influences γ (from 74.49° to 292.23°) by changing the location of the body bending point and the head impact point on the vehicle.

4.2. The influence mechanism of bonnet angle on rotation angle

Fig. 10 illustrates the detailed kinematic response processes of pedestrians struck by vehicles with varying α values while the other three parameters are maintained at baseline values at 40 km/h. When the extracted images are analyzed at 200 ms, the head impact point located on the bonnet tends to be higher with increasing bonnet angle α, thereby reducing the obstacle during the body rotation period. When α = 20°, 25°, 30°, the pedestrian rotates freely without any disturbance after the primary impact. In these cases, the generated γ is directly influenced by α. In particular, when struck by a vehicle with a larger α, the body rotates at a smaller angle before the instant of head–vehicle impact, which leads to a smaller rotation angle at any subsequent time, and eventually, a smaller γ. When α = 5°, 10°, 15°, the additional obstacle effect causes γ to vary irregularly. In general, α influences γ (from 92.25° to 232.64°) only by changing the location of the impact point between the head of the pedestrian and the vehicle. Consequently, the sensitivity of γ to α is lower than that to H.

4.3. The influence mechanism of bonnet length and windscreen angle on rotation angle

Figs. 11 depicts the pedestrian kinematic response processes. The vehicle front-end shape varies with L, whereas the other three parameters are maintained at baseline values. As shown in Fig. 11, particularly the images

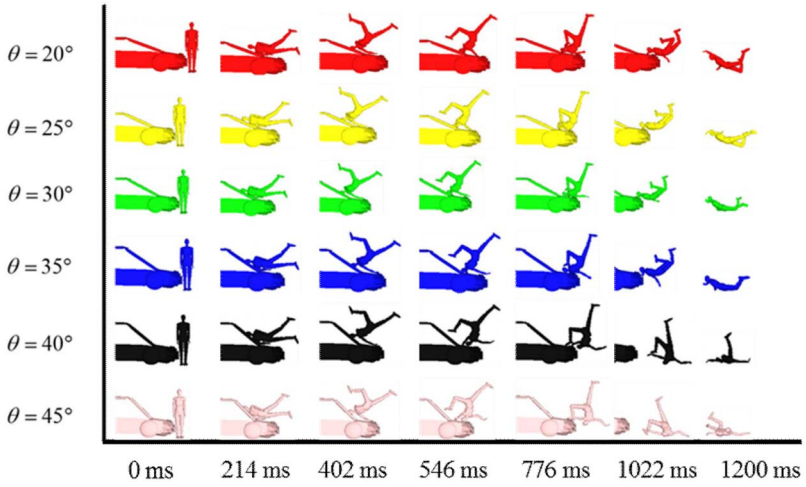

Fig. 7. Six kinematic processes of pedestrians struck by vehicles with a constant H of 0.6 m and different θ values at 30 km/h. The α and L of the six vehicles are maintained at baseline values.

Table 2
The significance levels of vehicle front-end design factors on rotation angle at 40 km/h.

Coupling variables	Source of variation	P-value
H, α	*H*	5.72E-10
	α	0.057
H,L	*H*	8.61E-21
	L	0.86
H, θ	*H*	2.7E-15
	θ	0.68

Table 3
Estimated coefficients and p-values for regression model.

	Fitted regression coefficient	Std. error	p-Value
Baseline	337.887		
H	−2.066	0.804	0.012
α	0.037	0.026	0.634
L	0.236	0.495	0.167
θ	0.008	0.017	0.626

at 118 ms, the head–vehicle impact point evidently moves from the windshield to the bonnet as *L* increases, whereas the horizontal distance between the impact point and the bonnet leading edge remains nearly unchanged, which results in a similar obstacle effect. Thus, the value of γ (from 76.21° to 91.68°) nearly remains constant. The sensitivity of γ to *L* is undeniably lower than those to *H* and α.

Six cases at 40 km/h (the vehicle front-end shape varies with *θ* while the other three parameters are maintained at baseline values) are selected to further investigate the influence mechanism of *θ*. The images at 116 ms in Fig. 12 show that a larger windshield angle (*θ*) slightly raises the head–vehicle impact point, which scarcely influences the subsequent kinematic process, and eventually generates a similar γ (44.69°–90.53°). Similarly, the fluctuation caused by *θ* in all the cases is always minimal except for the aforementioned special cases (*H* = 0.6 m, *θ* is approximately 40°). The sensitivity of γ to *θ* is evidently lower than those to *H* and α.

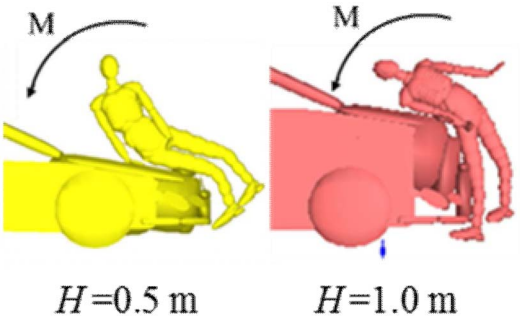

Fig. 9. Schematic view of the influence of *H* on the body bending point. The two images are extracted from the cases of *H* = 0.6 m and *H* = 0.1 m at 86 ms in Fig. 8.

4.4. Relationship between ground impact posture and ground impact injury

The influence mechanism of the dimensional parameters on impact

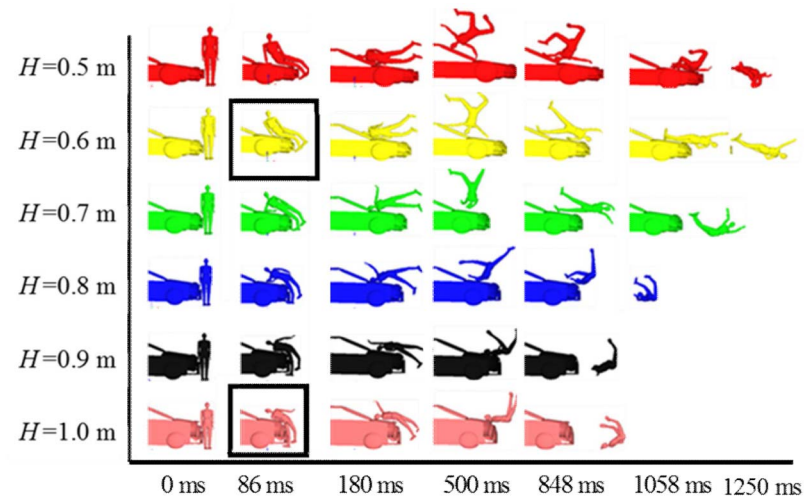

Fig. 8. Six kinematic processes of pedestrians struck by baseline vehicles with varying H values at 40 km/h. The images at 86 ms indicate the difference between the impact point and the body bending point.

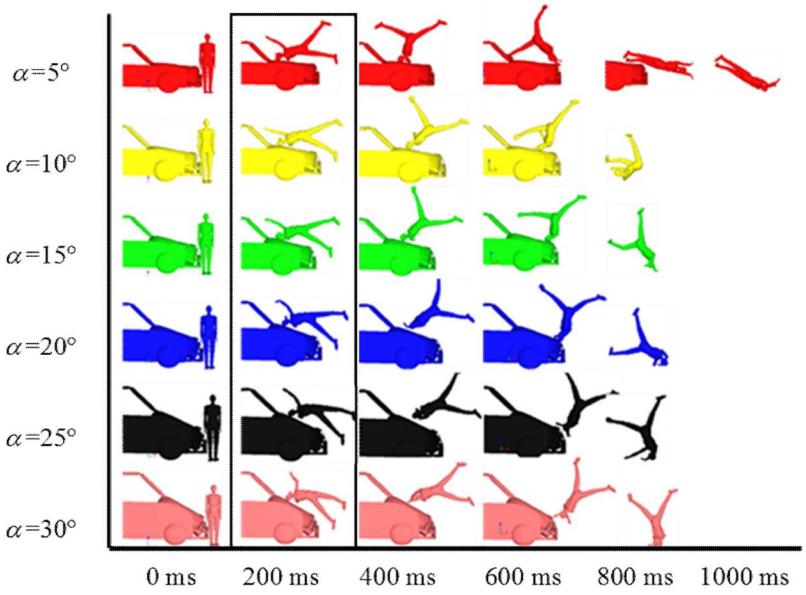

Fig. 10. Six kinematic processes of pedestrians struck by baseline vehicles with varying α values at 40 km/h. The images at 200 ms indicate the difference in impact point.

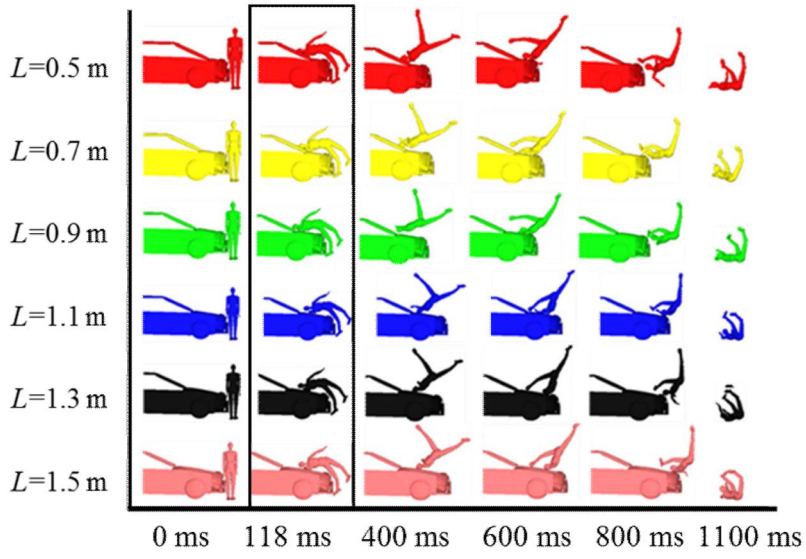

Fig. 11. Six kinematic processes of pedestrians struck by baseline vehicles with varying L values at 40 km/h. The images at 118 ms indicate the difference in impact point.

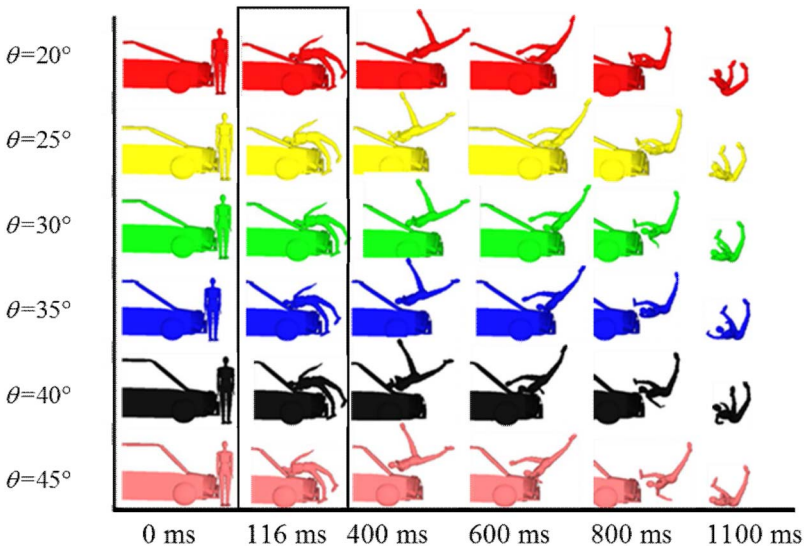

Fig. 12. Six kinematic processes of pedestrians struck by baseline vehicles with varying θ values at 40 km/h. The images at 116 ms indicate the difference in impact point.

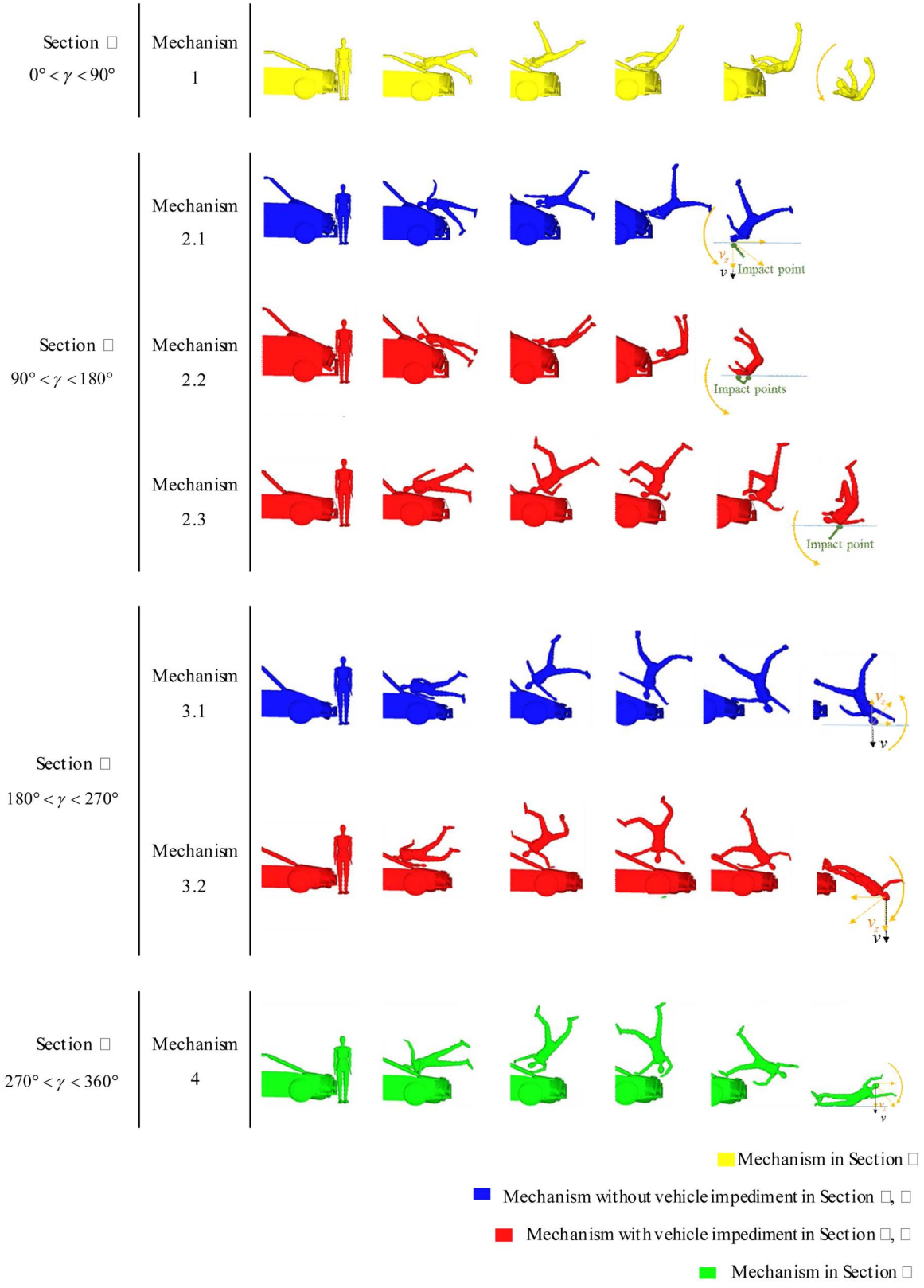

Fig. 13. Description of the seven identified mechanisms. Yellow indicates the mechanism in Section I, blue indicates the mechanisms without vehicle impediment in Sections II and III, red indicates the mechanisms with vehicle impediment in Sections II and III, and green indicates the mechanism in Section IV. (For interpretation of the references to colour in this figure legend, the reader is referred to the web version of this article.)

posture has been intensively studied, whereas the relationship between impact posture and head injury remains unclear. In this section, all the cases are further analyzed to probe into the relation between impact posture (γ) and head injury from secondary impact (HIC_{15}). As previously mentioned, all the cases can be divided into four categories based on the value of γ. Furthermore, seven detailed mechanisms in the four sections were proposed according to pedestrian impact gesture, as presented in Fig. 13. And the result of Kruskal-Wallis test revealed the

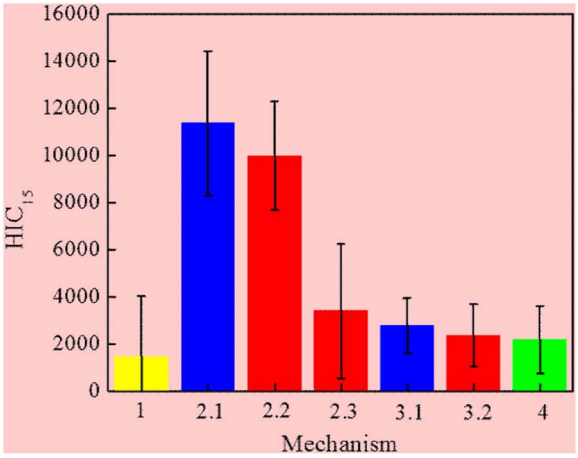

Fig. 14. Average values and standard deviations of HIC_{15} for each mechanism.

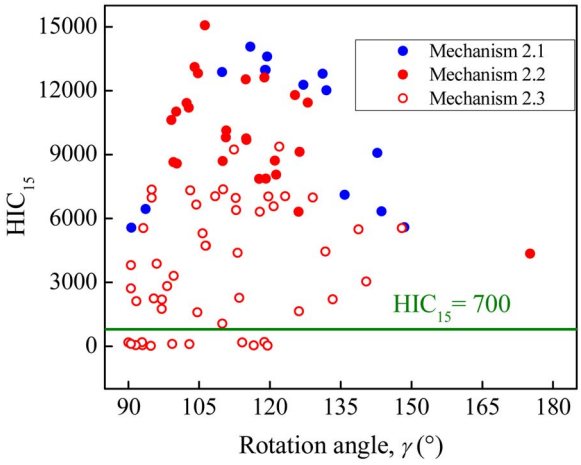

Fig. 15. HIC_{15} against rotation angle γ in Section II for three mechanisms. The dark blue rigid points indicate Mechanism 2.1 cases, the red rigid points indicate Mechanism 2.2 cases, and the red hollow points indicate Mechanism 2.3 cases. HIC_{15} = 700 is an agreement where with a low probability a fatality can occur. (For interpretation of the references to colour in this figure legend, the reader is referred to the web version of this article.)

statistical significance difference between seven mechanisms ($P < 0.001$). As shown in Fig. 14, Mechanisms 2.1 and Mechanisms 2.2 cases generate significantly higher average HIC value, i.e. $\overline{HIC}_{15}$ = 11348.3, 9990.0, respectively than those in Mechanisms 1 ($\overline{HIC}_{15}$ = 1480.7), Mechanisms 2.3 ($\overline{HIC}_{15}$ = 3409.0), Mechanisms 3.1 ($\overline{HIC}_{15}$ = 2767.7), Mechanisms 3.2 ($\overline{HIC}_{15}$ = 2359.4) and Mechanisms 4 ($\overline{HIC}_{15}$ = 2190.9) cases.

In Section I, pedestrians rotate less than 90° before coming in contact with the ground. The pelvis or legs hit the ground first, thereby mitigating head–ground contact to a certain extent and generating the lowest HIC_{15} value among the four sections (Fig. 14).

In Section II, pedestrians rotate between 90° and 180° before coming in contact with the ground, and rotation toward the ground intensifies head impact. As shown in Fig. 13, the 104 cases in Section II can be further divided into three sub-mechanisms, i.e., 21 cases (20.19%) of Mechanism 2.1, 26 cases (25.00%) of Mechanism 2.2, and 57 cases (54.81%) of Mechanism 2.3. As mentioned earlier, Mechanisms 2.1 and Mechanisms 2.2 cases generate significantly higher $\overline{HIC}_{15}$ = 11348.3 and 9990.0 than Mechanisms 2.3 ($\overline{HIC}_{15}$ = 3409.0). The three mechanisms are statistically distinct in HIC_{15} distribution because of the difference in impact points. In Mechanism 2.1, pedestrians rotate without interference from the vehicle front-end and finally hit the ground directly on their head, generating the highest HIC_{15} among the three mechanisms in Section II, as shown in Fig. 15. In Mechanism 2.2, the head of the pedestrians are impeded by the vehicle leading edge at the instant of separation, thereby causing the neck to flex slightly toward the chest. Finally, the shoulders and the head come in contact with the ground nearly at the same instant and absorb the ground impact together. The HIC_{15} value of Mechanism 2.2 belongs to superior middling, as shown in Fig. 15. A strong interference between the head of the pedestrian and the vehicle occurs during the pedestrian rotation period in Mechanism 2.3. In these circumstances, the flexion of the neck is extremely severe such that only the shoulders strike the ground and protect the head as a buffer. The HIC_{15} value of Mechanism 2.3 is the lowest (Fig. 15).

In Section III, pedestrians rotate between 180° and 270° before coming in contact with the ground. In addition, nearly all the cases occur with the head coming directly in contact with the ground, but the HIC_{15} value (2499.5) is not as high as that in Section II. To explain this phenomenon, the 30 cases in Section III are divided into two sub-mechanisms (Fig. 13), namely, 19 cases (63.33%) of Mechanism 3.1 and 11 cases (36.67%) of Mechanism 3.2. In Mechanism 3.1, pedestrians rotate without interference from the vehicle front-end until the head comes in contact with the ground. In these cases, the rotation away from ground generates a vertical component v_z opposite to the impact velocity v at the instant of ground impact, thereby weakening head impact severity. Furthermore, as shown in Fig. 16(a), a linear fit between HIC_{15} and γ yields a high correlation (R^2 = 0.44) in Mechanism 3.1. A larger γ (180°–270°) generally yields a lower HIC_{15} value because of the effect of a larger v_z. In Mechanism 3.2, the pedestrian first rotates nearly 270° until he or she is lying flat on the vehicle front-end. Thereafter, the upper body rotates toward the ground because of gravity, whereas the lower limbs are impeded by the vehicle, this period is named secondary rotation. Finally, the head of the pedestrian hits the ground. In these cases, the injury is not extremely severe because the buffering action of the vehicle front-end significantly impedes the first rotation period. Consequently, injury is mainly determined by the secondary rotation period, which highly depends on H. As shown in Fig. 17(b), in the case of Mechanism 3.2, a higher H generates a smaller γ (R^2 = 0.31) and a higher HIC_{15} (R^2 = 0.65) because more secondary rotations occur. The relationship between H and γ is not strict linear so the value of R^2 is low.

In Section IV, pedestrians rotate more than 270° before hitting the ground. After the contact between the pelvis and the ground, a pedestrian reverses the rotation direction and rotates toward the ground. The buffering action of the pelvis significantly reduces the severity of the injury.

4.5. Relationship between dimensional parameters and ground impact injury

Figs. 15 and 16(a) show that no explicit relationship can be drawn between γ and HIC_{15} because of the diversity of mechanisms resulting from the impediment of the vehicle. Consequently, although the relationship between the dimensional parameters and γ is apparent, determining the influencing mechanism of the dimensional parameters on HIC_{15} remains difficult.

Fig. 17 illustrate the coupling effect of H and the other three dimensional parameters (α, L, and θ) on HIC_{15}, respectively. The variation in HIC_{15} is highly irregular with the change in dimensional parameters. This phenomenon can be explained by the complicated relationship between γ and HIC_{15}. Most importantly, since the used pedestrian model is not yet validated during the interaction with the ground, we tend to focus on the variation trend of injury outcome rather than absolute value. Some trends can be drawn out from Fig. 17 and provide solid guideline for vehicle safety design within limitations of this study. Firstly, with a higher impact velocity, vehicle front-end shapes tends to play a larger role in influencing head-ground impact injury. Secondly, for the present investigation conditions, vehicles with

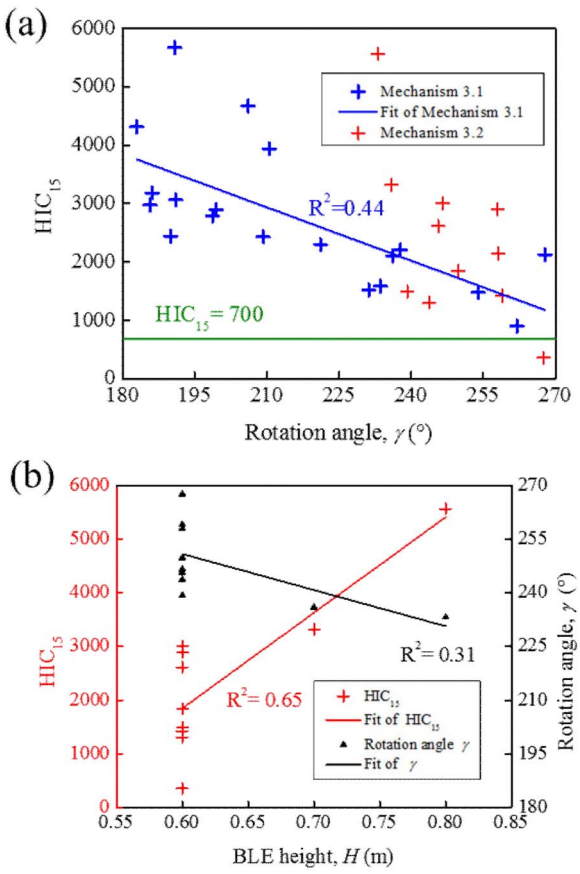

Fig. 16. (a) HIC_{15} against rotation angle γ in Section III for two mechanisms. The dark blue crosses indicate Mechanism 3.1 cases, and the red crosses indicate Mechanism 3.2 cases. The dark blue line is the fitting curve of Mechanism 3.1 cases. HIC_{15} = 700 is an agreement where with a low probability a fatality can occur. (b) Relation among γ, HIC_{15}, and H for Mechanism 3.2 cases. The red crosses indicate HIC_{15} = 700, and the black crosses indicate γ. (For interpretation of the references to colour in this figure legend, the reader is referred to the web version of this article.)

bonnet-leading edge height of 1.0 m tend to be more aggressive for pedestrian at a velocity of 40 km/h. Thirdly, among the four dimensional parameters, the head-ground injury are more sensitive to H,α than L and θ.

The aforementioned analysis all focus on the coupling effect of two dimensional parameters on HIC_{15}. For a more comprehensive analysis of this problem, multiple linear regression analysis for HIC_{15} (outcome variable) using four dimensional parameters as explanatory variables has been made based on cases at 40 km/h. The following is the regression model:

$$HIC_{15} = \beta_0 + \beta_H H + \beta_\alpha \alpha + \beta_L L + \beta_\theta \theta \quad (2)$$

Table 4 lists brief information on the fitted coefficients and p-values for the variables in the regression model. It is worth to note that the significant levels of H,α,L,θ are 0.000, 0.125, 0.183,0.345 respectively. In the presence of H, the other variables α,L,θ are not statistical significant.

4.6. Limitations of the study

Validated stiffness and contact characteristics were applied to the impact model and played an essential role in pedestrian kinematics. However, they did not account for differences in stiffness and characteristic between vehicle types. In addition, the effect of vehicle weight was not analyzed, and it has some effect on pedestrian kinematics.

A 50th percentile male model was used in this study. Different

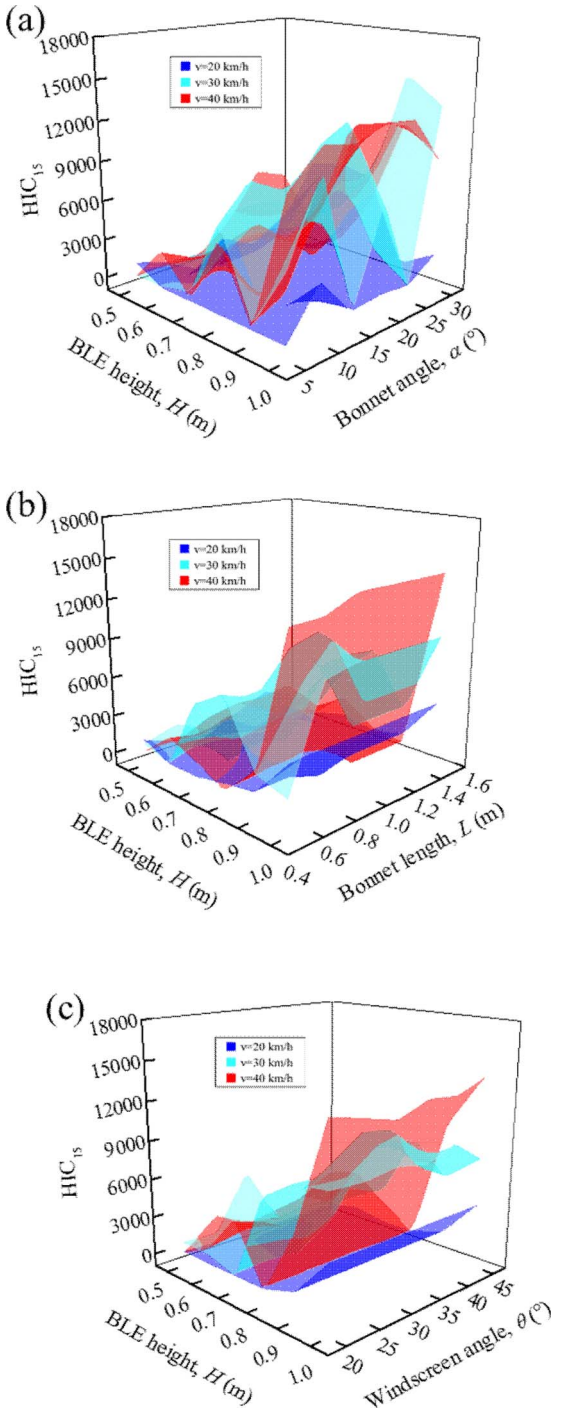

Fig. 17. (a) Coupling effect of H and α on HIC_{15} at all impact speeds (20, 30, and 40 km/h). (b) Coupling effect of H and L on HIC_{15} at all impact speeds (20, 30, and 40 km/h). (c) Coupling effect of H and θ on HIC_{15} at all impact speeds (20, 30, and 40 km/h). The red, light blue, and dark blue surfaces represent the cases at 40, 30, and 20 km/h, respectively. (For interpretation of the references to colour in this figure legend, the reader is referred to the web version of this article.)

Table 4
Estimated coefficients and p-values for regression model.

	Fitted regression coefficient	Std. error	p-Value
Baseline	−11332.409		
H	19569.452	1869.560	< 0.001
α	94.897	61.367	0.125
L	−1544.749	1151.552	0.183
θ	37.132	39.123	0.345

pedestrian sizes would have a significant influence on the results due to different bonnet height/pedestrian height ratios. An assumption was made that the impact point between the pedestrian and vehicle is at the middle section of the vehicle especially at lower velocities where the pedestrian may be alerted but does not have time to clear impact.

Most importantly, the MADYMO pedestrian model is not yet validated for the prediction of head injuries from the impact with the ground.

5. Conclusions

Head–ground impact is the primary cause of head injuries in pedestrian–vehicle accidents. To probe into the influences of vehicle front-end dimensional parameters on head injuries during secondary impact, bonnet leading edge height (H), bonnet angle (α), bonnet length (L), and windshield angle (θ) are selected as the main dimensional parameters that can briefly evaluate the profile of vehicle front-end. Parametric vehicle front-ends are generated based on the parametric matrix of these four variables in the MADYMO platform to simulate the collisions at three different velocities. However, the capability of the pedestrian model to predict injury from ground impact has not been verified. To address this limitation, focus should be directed more toward the general trends of the results rather than toward specific data. The following conclusions can be drawn from the study.

- The variation in rotation angle (γ) arising from H and all the three parameters tends to be larger with a higher impact velocity. At 20 km/h, γ is observed only in Sections I and II. At 30 km/h, γ is observed in Sections I, II, and III. At 40 km/h, the value range of γ expands to Sections I, II, III, and IV. A high impact velocity can magnify the influences of dimensional parameters on rotation angle.
- At 40 km/h, H dominates ground impact posture by changing the positions of the body bending point and the head–vehicle impact point. By contrast, α, L, and θ only make a difference in the head–vehicle impact point. The variation caused by α is more conspicuous than those caused by L and θ.
- The relationship between γ and HIC_{15} is complicated because of the involvement of the vehicle front-end shape during the pedestrian rotation period. Accordingly, seven detailed mechanisms in the four sections are suggested. Among these mechanisms, Mechanism 2.1 in Section I generates the highest HIC_{15}.
- Vehicles with bonnet-leading edge height of 1.0 m tend to be more aggressive for pedestrian at a velocity of 40 km/h within the limitations of the study.

The results may provide informative head–ground impact injury mechanisms which are meaningful for head-ground impact research. While considering the safety of pedestrian into vehicle safety design, the conclusions can serve as a solid guideline within limitations of this study.

Acknowledgement

This work is financially supported by start-up funds of “The Recruitment Program of Global Experts” awardee from Beihang University (YWF-16-RSC-011) andBeijing Municipal Science & Technology Commission (Grant No. Z161100001416006).

References

Automotive, T., 2013. Manual: Madymo Human Body Models. Delft, The Netherlands.
Belingardi, G., Chiandussi, G., 2011. Vehicle crashworthiness design — general principles and potentialities of composite material structures. In: Abrate, S. (Ed.), Impact Engineering of Composite Structures. Springer, Vienna, Vienna, pp. 193–264.
Crocetta, G., Piantini, S., Pierini, M., Simms, C., 2015. The influence of vehicle front-end design on pedestrian ground impact. Accid. Anal. Prev. 79, 56–69.
Cuerden, R., Richards, D., 2007. Pedestrians and Their Survivability at Different Impact Speeds.
Demarco, A.L., Chimich, D.D., Gardiner, J.C., Siegmund, G.P., 2016. The impact response of traditional and bmx-style bicycle helmets at different impact severities. Accid. Anal. Prev. 92, 175–183.
EEVC, 1998. Improved Test Methods to Evaluate Pedestrian Protection Afforded by Passenger Cars. EEVC Working Group 17 Report.
Elliott, J.R., Simms, C.K., Wood, D.P., 2012. Pedestrian head translation, rotation and impact velocity: the influence of vehicle speed, pedestrian speed and pedestrian gait. Accid. Anal. Prev. 45 (1), 342–353.
Euro-NCAP, 2013. European New Car Assessment Programme Pedestrian Testing Protocol, Version 4.3.
Feng, C.J., Wang, F.P., Chen, X.U., Wei, F., Liu, S.X., Yin, Z.Y., 2013. Head dynamic response based on reconstruction of vehicle-pedestrian accidents with the video. Yiyong Shengwu Lixue/journal of Medical Biomechanics 28 (2), 164–170.
Gupta, V., Yang, K.H., 2013. Effect of vehicle front end profiles leading to pedestrian secondary head impact to ground. Stapp Car Crash J. 57 (57), 139–155.
Hamacher, M., Eckstein, L., Paas, R., 2012. Vehicle related influence of post-car impact pedestrian kinematics on secondary impact. Proceedings of the IRCOBI Conference Proceedings.
Han, Y., Yang, J., Mizuno, K., Matsui, Y., 2011. Effects of vehicle impact velocity on pedestrian fatal injury risk. Chin. J. Automot. Eng. 1 (4).
Han, Y., Yang, J., Mizuno, K., Matsui, Y., 2012. Effects of vehicle impact velocity, vehicle front-end shapes on pedestrian injury risk. Traffic Inj. Prev. 13 (5), 507–518.
Hefny, A.F., Eid, H.O., Abuzidan, F.M., 2014. Pedestrian injuries in the united arab emirates. Int. J. Injury Control Saf. Promotion 22 (3), 203–208.
Iwamoto, M., Kisanuki, Y., Watanabe, I., Furusu, K., Miki, K., Hasegawa, J., 2002. Development of a finite element model of the total human model for safety (thums) and application to injury reconstruction. Proceedings of the PROCEEDINGS OF THE INTERNATIONAL IRCOBI CONFERENCE.
Kendall, R., Meissner, M., Crandall, J., 2006. The causes of head injury in vehicle-pedestrian impacts: comparing the relative danger of vehicle and road surface. Proceedings of the SAE 2006 World Congress Exhibition.
Kerrigan, J., Kam, C., Drinkwater, C., Murphy, D., Bose, D., Ivarsson, J., Crandall, J., 2005. Kinematic Comparison of the Polar-ii and Pmhs in Pedestrian Impact Tests with a Sport-utility Vehicle.
Kerrigan, J., Arregui-Dalmases, C., Crandall, J., 2012. Assessment of pedestrian head impact dynamics in small sedan and large suv collisions. Int. J. Crashworthiness 17 (3), 243–258.
Lyons, M., Simms, C.K., 2012. Predicting the influence of windscreen design on pedestrian head injuries. Proceedings of the IRCOBI ConferenceIRCOBI Conference.
Martinez, L., Guerra, L.J., Ferichola, G., Garcia, A., 2007. Stiffness corridors of the european fleet for pedestrian simulation. Proceedings of the Experimental Safety Vehicles Conference.
Mizuno, K., Yonezawa, H., 2001. Pedestrian headform impact tests for various vehicle locations. J. Jpn. Lang. Stud. Res.
K. Oida G., Kobayashi K., Mizuno D., Ito 2d26 the study on head protection with cyclist helmet in impact against vehicle a-pillar,
バイオエンジニアリング講演会講演論文集, 264, 865–868, (2015).
Otte, D., Pohlemann, T., 2001. Analysis and Load Assessment of Secondary Impact to Adult Pedestrians After Car Collisions on Roads.
Poorfakhraei, A., Samimi, A., Ermagun, A., 2014. Investigating the effect of impact speed on pedestrian fatality in traffic accidents using a hazard based duration model. Proceedings of the Transportation Research Board 93rd Annual Meeting.
Roudsari, B.S., Mock, C.N., Kaufman, R., 2005. An evaluation of the association between vehicle type and the source and severity of pedestrian injuries. Traffic Inj. Prev. 6 (2), 185–192.
Sankarasubramanian, H., Chawla, A., Mukherjee, S., Goehlich, D., 2015. Optimisation study on multibody vehicle-front model for pedestrian safety. Int. J. Crashworthiness 21 (1), 63–78.
Simms, C.K., Wood, D.P., 2006. Effects of pre-impact pedestrian position and motion on kinematics and injuries from vehicle and ground contact. Int. J. Crashworthiness 11 (11), 345–355.
Simms, C., Wood, D., 2009. Pedestrian and cyclist impact. Solid Mech. Appl. 166, 31–49.
Simms, C.K., Ormond, T., Wood, D.P., 2011. The Influence of Vehicle Shape on Pedestrian Ground Contact Mechanisms.
Subit, D., Kerrigan, J., Crandall, J., 2008. Pedestrian-vehicle Interaction: Kinematics and Injury Analysis of Four Full Scale Tests. pp. 67–81.
WHO, 2015. Who Global Status Report on Road Safety 2015. World Health Organization ed.
Wood, D., Simms, C., Wood, D., 2000. Coefficient of friction in pedestrian throw. Impact J.ITAI 9 (1), 12–14.
Xu, J., Shi, S., Yu, G., Qi, H., Wang, Y., Xu, S., 2015. Are electric self-balancing scooters safe in vehicle crash accidents? Accid. Anal. Prev. 87, 102–116.
Xu, J., Shi, S., Qi, H., Yu, G., Wang, Y., Chen, P., 2016. Simulative investigation on head injuries of electric self-balancing scooter riders subject to ground impact. Acci. Anal. Prev. 89, 128–141.
Yan, X., Ma, M., Huang, H., Abdel-Aty, M., Wu, C., 2011. Motor vehicle-bicycle crashes in beijing: irregular maneuvers, crash patterns, and injury severity. Accid. Anal. Prev. 43 (5), 1751–1758.
Yan, W., Xu, X., Liu, B., Xu, J., Li, Y., University, T., 2015. A study on the coupling

influence of impact speed and vehicle type on the movement and injury of pedestrian. Qiche Gongcheng/automotive Engineering 37 (3), 276–283.
Yang, J., Yao, J., 2005. Correlation of different impact conditions to the injury severity of pedestrians in real world accidents. Proceedings of the 19th International Technical Conference on the Enhanced Safety of Vehicles.
Yang, J.K., Lövsund, P., Cavallero, C., Bonnoit, J., 2000. A human-body 3d mathematical model for simulation of car-pedestrian impacts. Crash Prev. Injury Control 2 (2), 131–149.
Yao, J., Yang, J., Otte, D., 2008. Investigation of head injuries by reconstructions of real-world vehicle-versus-adult-pedestrian accidents. Saf. Sci. 46 (7), 1103–1114.